Plant Direct

WILEY

American Society of Plant Biologists SEB SOCIETY FOR EXPERIMENTAL BIOLOGY

RESEARCH ARTICLE OPEN ACCESS

The Atypical Pectin Methylesterase Family Member PME31 Promotes Seedling Lipid Droplet Utilization

Sarah Hamade | Melissa S. Traver | Bonnie Bartel

Biosciences Department, Rice University, Houston, Texas, USA

Correspondence: Bonnie Bartel (bartel@rice.edu)

Received: 2 August 2024 | **Revised:** 14 December 2024 | **Accepted:** 4 January 2025

Funding: This work was supported by the National Institutes of Health (R35GM130338) and the Robert A. Welch Foundation (C-1309). Whole-genome sequencing was performed by The Genome Technology Access Center at Washington University School of Medicine, which is partially supported by an NIH National Cancer Institute Cancer Center Support Grant (P30CA91842) and the NIH National Center for Research Resources ICTS/CTSA (UL1TR002345). Lipid analyses were performed at the Kansas Lipidomics Research Center Analytical Laboratory, where instrument acquisition and lipidomics method development were supported by the National Science Foundation (including the Major Research Instrumentation program; DBI-1726527), K-IDeA Networks of Biomedical Research Excellence (INBRE) of National Institute of Health (P20GM103418), USDA National Institute of Food and Agriculture (Hatch/Multi-State project 7001195), and Kansas State University. Structure visualization used UCSF ChimeraX, which was developed by the Resource for Biocomputing, Visualization, and Informatics at the University of California, San Francisco, with support from the National Institutes of Health R01-GM129325 and the Office of Cyber Infrastructure and Computational Biology at the National Institute of Allergy and Infectious Diseases.

Keywords: *Arabidopsis* germination | lipid droplet | lipid mobilization | oleosin | pectin methylesterase | peroxisome

ABSTRACT

In plants, the primary form of energy stored in seed lipid droplets, triacylglycerol (TAG), is catabolized during germination to support pre-photosynthetic growth. Although this process is essential for seedling development, it is incompletely understood. In a screen for *Arabidopsis thaliana* mutants displaying delayed degradation of the lipid droplet coat protein oleosin, five independent mutations in *PECTIN METHYLESTERASE31* (*PME31*) were recovered. In addition to delayed oleosin degradation, *pme31* mutant seedlings exhibited sustained lipid droplets and elevated levels of several TAG and diacylglycerol species. Although structural prediction classified PME31 as a pectinesterase, this structural family also includes a putative *E. coli* lipase, YbhC. Moreover, PME31 lacks an N-terminal signal peptide that would target it to the cell wall, where pectin resides. We found that a fluorescent PME31 reporter was cytosolic and partially associated with peroxisomes, the site of fatty acid catabolism, during lipid mobilization. Our findings suggest that, in contrast to canonical PMEs, which modify cell wall pectin, PME31 functions at peroxisomes to directly or indirectly promote lipid mobilization.

1 | Introduction

Seed development is a fine-tuned process that directs embryo development and stockpiles energy resources to fuel eventual germination. In oilseed plants such as *Arabidopsis*, lipids are the primary fixed carbon source for germinating seeds before photosynthesis is established (Quettier and Eastmond 2009; Huang 1992). Utilization of these lipids requires the collaboration of two organelles—peroxisomes and lipid droplets.

Peroxisomes are found in nearly all eukaryotes, where they compartmentalize various catabolic and anabolic reactions essential for plant and animal life (Kao et al. 2018; Jansen et al. 2021; Kumar et al. 2024). For example, peroxisomes are the exclusive site of fatty acid β-oxidation in plants (Graham 2008). The enzymes that execute peroxisome functions are synthesized in the cytosol and imported into the lumen of the organelle using a suite of proteins known as peroxins (PEX proteins) (Kao et al. 2018; Jansen et al. 2021). Lumenal proteins contain

Sarah Hamade and Melissa S. Traver contributed equally to this work.

a C-terminal peroxisomal targeting signal 1 (PTS1) and/or a PTS2 near the N-terminus. These signals are recognized by the import receptors PEX5 and PEX7, respectively, that accompany the cargo proteins through PEX13 hydrogel channels into the lumen of the peroxisome (Gao et al. 2022; Ravindran et al. 2023; Skowyra et al. 2024). After cargo delivery, the receptors are retrotranslocated out of the peroxisome through the action of ubiquitination and ATPase peroxin complexes on the peroxisome membrane, freeing the receptors for further rounds of import (Kao et al. 2018; Jansen et al. 2021).

The fats catabolized in peroxisomes are stored in lipid droplets (also known as oil bodies) to prevent cytotoxicity. Lipid droplets are dynamic, ER-derived organelles with a neutral lipid core of triacylglycerol (TAG) and steryl esters surrounded by a phospholipid monolayer (Choudhary et al. 2015; Jacquier et al. 2011; Kassan et al. 2013). The lipid droplet membrane is embedded with coat proteins, including oleosin in plants, to maintain structural integrity and prevent lipid droplet coalescence (Walther et al. 2017; Huang 1992).

During germination, lipid droplets deliver lipids to peroxisomes for utilization. To allow access to the stored lipids, the oleosin coat proteins are ubiquitinated, which requires a peroxisome-associated ubiquitin-protein ligase, MIEL1 (Traver and Bartel 2023). Ubiquitinated oleosins are extracted from the lipid droplet membrane by the ATPase CDC48, assisted by the adaptor protein PUX10 (Deruyffelaere et al. 2018; Kretzschmar et al. 2018), and degraded by the proteasome (Deruyffelaere et al. 2015). Fatty acids stored in lipid droplet TAG are released as peroxisomal extensions known as peroxules emerge from the peroxisome to allow SUGAR DEPENDENT1 (SDP1), a cytosol-facing TAG lipase anchored in the peroxisomal membrane, to access the surface of the lipid droplet (Thazar-Poulot et al. 2015; Huang et al. 2022). SDP1 hydrolyzes TAG into a free fatty acid and diacylglycerol (DAG) and can also inefficiently remove a second fatty acid from DAG to produce monoacylglycerol (MAG) (Eastmond 2006). The esterification of the freed fatty acid to CoA allows the resultant fatty acyl-CoA to be imported into the peroxisome by the ABC transporter PXA1 (Zolman et al. 2001; Footitt et al. 2002), which hydrolyzes the CoA during transport (De Marcos Lousa et al. 2013; Carrier et al. 2019). Inside the peroxisome, the fatty acid is again esterified to CoA (Fulda et al. 2004) to ready it for the β-oxidation spiral, which is catalyzed by the sequential action of acyl-CoA oxidases (ACX enzymes) (Adham et al. 2005), multifunctional enzymes (AIM1 and MFP2) (Rylott et al. 2006), and 3-ketoacyl-CoA thiolases (PED1, KAT1, and KAT5) (Hayashi et al. 1998; Wiszniewski et al. 2014). Each cycle of the fatty acid β-oxidation spiral releases acetyl-CoA, which supplies the glyoxylate cycle to produce the sucrose that fuels germination (Graham 2008; Theodoulou and Eastmond 2012).

Arabidopsis mutants defective in lipid mobilization often display seedling growth defects that can be ameliorated by supplementing the growth medium with sucrose. Providing this alternative fixed carbon source bypasses the need for acetyl-CoA from fatty acid β-oxidation. These mutants include *sdp1*, which inefficiently hydrolyzes TAG (Thazar-Poulot et al. 2015; Eastmond 2006); *pxa1*, which ineffectively imports fatty acids into peroxisomes (De Marcos Lousa et al. 2013; Carrier et al. 2019); and *ped1*, which is defective in a thiolase enzyme catalyzing the final step of β-oxidation (Hayashi et al. 1998). Another notable phenotype of lipid mobilization mutants is the clustering of peroxisomes around retained lipid droplets; *sdp1*, *pxa1*, *acx1*, *acx2*, *mfp2*, and *ped1* mutants emerged from a microscopy-based screen for seedlings with clustered or enlarged peroxisomes (Rinaldi et al. 2016). In addition to enzymes involved in processing and transporting lipids, the timely degradation of the lipid droplet coat protein oleosin (OLE) is needed for efficient lipid droplet utilization, and *miel1* and *pux10* mutants display slowed lipid droplet utilization during germination (Deruyffelaere et al. 2018; Kretzschmar et al. 2018; Traver and Bartel 2023).

Despite the importance of lipid mobilization for plant growth, several aspects of this process remain unclear. For example, several *Arabidopsis* mutants defective in PECTIN METHYLESTERASE31 (PME31) emerged from the same microscopy-based screen that also revealed multiple lipid mobilization mutants (Rinaldi et al. 2016). As PMEs typically act in the plant cell wall to demethylate pectin (Micheli 2001), it is not apparent why *pme31* mutants would exhibit lipid mobilization defects. In this study, we identified five new *pme31* alleles in a screen for delayed oleosin degradation during *Arabidopsis* seed germination. We found that levels of prominent neutral lipids, including DAG and some TAG species, were elevated in *pme31* mutant seedlings. Additionally, a PME31 reporter expressed from the *PME31* promoter localized to the cytosol until robust lipid mobilization began, when it was also found associated with peroxisomes. These findings establish PME31 as an atypical PME that plays a key role in lipid mobilization in *Arabidopsis*.

2 | Results

2.1 | Multiple *pme31* Alleles Emerged From a Screen for Delayed Oleosin Degradation

To identify proteins involved in lipid mobilization, we isolated mutants with delayed degradation of the predominant seedling lipid droplet coat protein OLEOSIN1 (OLE1) during seedling development. We used ethyl methanesulfonate (EMS) to mutagenize an *Arabidopsis* line containing a transgene (*pOLE1:mNeonGreen-OLE1*) that expressed an mNeonGreen-OLE1 translational fusion from the *OLE1* promoter (Traver and Bartel 2023). As previously described (Traver and Bartel 2023), we screened the progeny of these plants for delayed mNeonGreen-OLE1 degradation by using fluorescence microscopy to identify mutant seedlings that retained mNeonGreen fluorescence after it was no longer prominent in wild-type seedlings (Figure 1A). We tested the progeny of our candidate mutant seedlings for sustained fluorescence by microscopy and for elevated endogenous and reporter oleosin levels by immunoblotting (Figure 1B), and we used whole-genome sequencing to identify homozygous EMS-consistent mutations (G-to-A or C-to-T) in our validated mutants. In addition to previously described mutations in the *MIEL1* gene, which encodes a ubiquitin-protein ligase (Traver and Bartel 2023), we identified five independent missense mutations in *PME31* (Figure 1C). Previously isolated *pme31* alleles respond like wild type to growth without sucrose or when challenged with the peroxisomally processed auxin

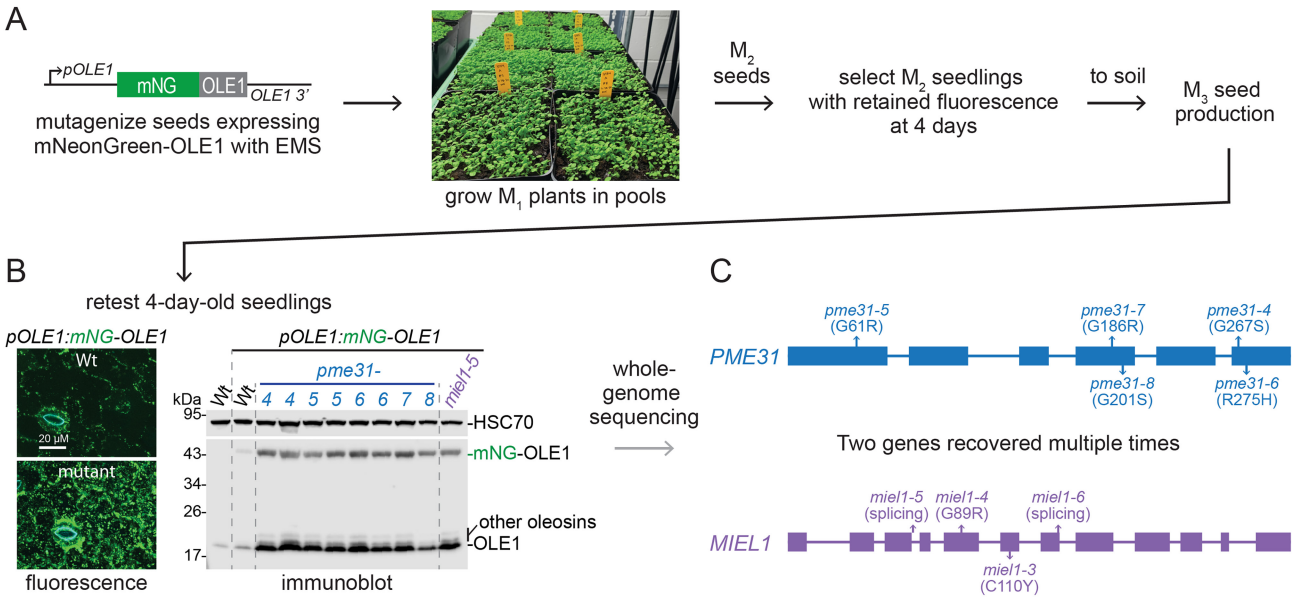

FIGURE 1 | A screen for oleosin stabilization uncovers multiple *pme31* alleles. (A) *pOLE1:mNeonGreen-OLE1* seeds were mutagenized and grown in pools, and their progeny (M_2) were screened for sustained seedling fluorescence and then transferred to soil for seed production. (B) Four-day-old M_3 seedlings were retested for mNeonGreen fluorescence (left) and protein stabilization via immunoblotting (right). An immunoblot of protein extracted from 4-day-old untransformed wild type (Wt), un-mutagenized *pOLE1:mNeonGreen-OLE1* (Wt), and *pme31* mutant seedlings was serially probed with antibodies recognizing seed oleosins and the HSC70 loading control. Biological replicates of the *pme31-4*, *pme31-5*, and *pme31-6* alleles were loaded in adjacent lanes. The positions of molecular mass markers (in kDa) are indicated at the left. (C) Whole-genome sequencing of select mutants revealed multiple independent alleles in two genes: *PME31* (blue; this work) and *MIEL1* (purple; Traver and Bartel 2023).

precursor, indole-3-butyric acid (IBA) (Rinaldi et al. 2016). Similarly, we found that all five of our *pme31* mutants resembled wild type in these conditions, which was in marked contrast to the peroxisome-defective *pex12-1* mutant (Figure S1) (Kao et al. 2016). Because all five *pme31* mutants emerged from the same screen for mNeonGreen-OLE1 retention (Figure 1), lacked seedling growth defects (Figure S1), and similarly stabilized endogenous oleosins (Figure 1B), we selected one allele, *pme31-5*, for in-depth analysis.

2.2 | PME31 Promotes Lipid Droplet Mobilization

To determine if the sustained oleosin observed in *pme31* was associated with lipid droplets, we investigated lipid droplet prominence during early seedling development. Using confocal microscopy, we observed abundant OLE1 reporter associated with lipid droplets stained with the neutral lipid dye monodansylpentane (MDH) in 2-day-old seedlings in both wild type and *pme31* (Figure 2A). By 4 days, both lipid droplets and the OLE1 reporter were largely depleted in wild type, whereas the *pme31* mutant displayed numerous residual lipid droplets associated with the OLE1 reporter (Figure 2A).

As observed in 4-day-old seedlings (Figure 1B), OLE1 and mNeonGreen-OLE1 levels were notably higher in 3-day-old *pme31* mutant seedlings compared to wild-type seedlings with or without the mNeonGreen-OLE1 reporter (Figure 2B). In contrast, *pme31* mutant seeds contained similar levels of OLE1 and mNeonGreen-OLE1 compared to wild-type seeds (Figure 2B). This time-course analysis suggested that rather than *pme31* seeds storing excess oleosin, oleosin degradation was delayed in the mutant. The accumulation pattern of the glyoxylate cycle enzyme isocitrate lyase (ICL), which is undetected in seeds, elevated in young seedlings, and degraded as seedlings are established (Lingard et al. 2009), was similar in *pme31* and wild type (Figure 2B), suggesting that PME31 did not notably impact the general timing of seedling development, which was consistent with our seedling growth assays (Figure S1).

We used thin-layer chromatography to examine the timing of TAG mobilization. We found similar levels of TAG in seeds and 1.5-day-old seedlings in *pme31* compared to wild type but significantly elevated TAG levels in 3.5-day-old *pme31* seedlings (Figure 2C,D). The slowed oleosin degradation and delayed mobilization of TAG and lipid droplets observed in the *pme31* mutant (Figure 2) suggest that PME31 promotes lipid mobilization.

2.3 | PME31 Influences Seedling DAG and TAG Levels

To understand how lipid mobilization is impacted in *pme31-5* compared to *miel1-4*, a lipid mobilization mutant that emerged from the same screen (Traver and Bartel 2023), we conducted lipid profiling on five biological replicates of 2-day-old light-grown seedlings. We included two controls: untransformed wild type and wild type expressing the mNeonGreen-OLE1 reporter that was also present in the two mutants. To examine the variation among our replicates and genotypes, we performed principal component analysis (PCA) (Figure 3A). We found that 96% of the variation in the data was captured by the first two principal components (Figure 3A). The replicates from the two control lines clustered together, indicating that

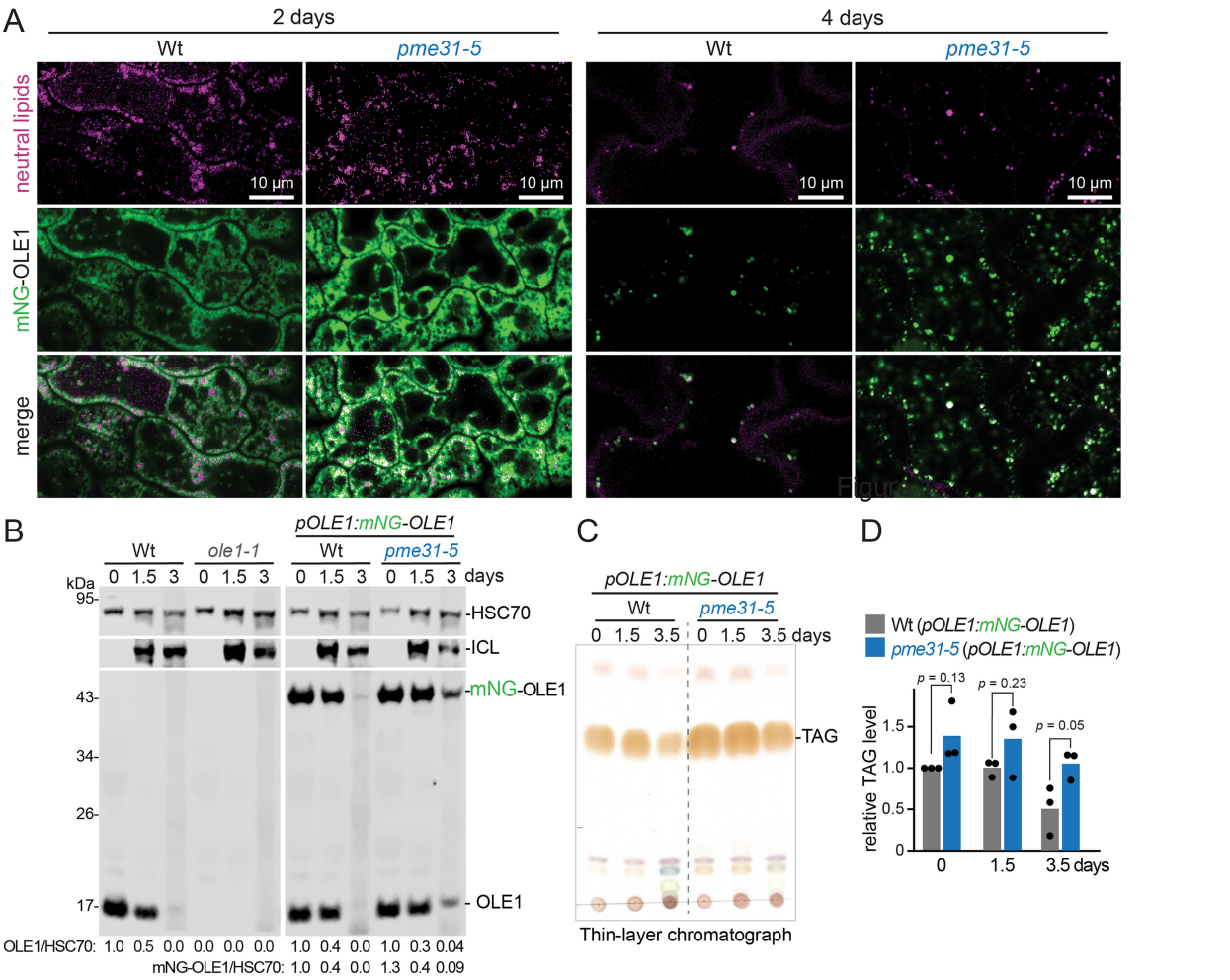

FIGURE 2 | *pme31* mutant seedlings retain lipid droplets, oleosin, and TAG longer than wild-type seedlings. (A) Confocal images (single slices) of cotyledon epidermal cells of Wt and *pme31-5* seedlings expressing mNeonGreen (mNG)-OLE1 at the indicated ages. Neutral lipids were stained with MDH (magenta), and mNG-OLE1 fluorescence is shown in green. (B) Immunoblot of protein extracted from stratified seeds (0 days) and 1.5- and 3-day-old seedlings probed with the indicated antibodies. The positions of molecular weight markers (in kDa) are indicated on the left. The numbers below the panels show the OLE1 or mNG-OLE1 to HSC70 ratio, normalized to the day 0 level in Wt or Wt (pOLE1:mNG-OLE1), respectively. (C) Representative thin-layer chromatograph (TLC) of extracted lipids of the indicated genotypes at 0-, 1.5-, and 3-day time points. (D) Quantification of triplicate TLC of the indicated genotypes. The TAG signal was standardized against wild type at 0 days for each replicate. *p*-values were generated by three individual two-tailed unpaired t-tests of the time-course groups.

the mNeonGreen-OLE1 transgene did not markedly impact overall lipid composition. In contrast, the data from the two mutants were well separated from each other and from the controls (Figure 3A), indicating distinct alterations in lipid composition.

Because our mutants emerged from a screen for lipid droplet retention, we analyzed the lipidomics data for changes in the lipids most notably associated with lipid droplets—TAG, DAG, and sterols. The most prominent differences between the mutants and the wild-type control expressing mNeonGreen-OLE1 were significant elevations in DAG levels; some TAG species were also significantly elevated (Figures 3B and S2). In contrast, sterol levels were not significantly altered in the mutants (Figure 3B,D). To examine the contribution of these altered lipids to the total seedling lipid content, we compared the levels of individual TAG (Figure 3C), DAG (Figure 3D), and sterol (Figure 3E) species for each genotype. We found that both *pme31* and *miel1* had elevated levels of the most abundant DAG species (18:2_18:2), whereas *pme31* but not *miel1* had elevated levels of the most abundant TAG species (18:2_36:3 and 18:2_36:4). Among changes in polar lipids, we noted that *pme31-5* and *miel1-4* appeared to have decreased levels of several monogalactosyldiacylglycerol (MGDG) species compared to the control (Figure S2).

2.4 | PME31 Is Unique Among *Arabidopsis* Pectin Methylesterases

To gain insight into why mutants defective in PME31, an apparent pectin methylesterase, might display delayed lipid mobilization, we probed bioinformatic data related to the homology and structure of PME31. Plant PMEs generally have one of two types of N-terminal extensions. Type I PMEs, exclusive to the Embryophyta (land plants), have an N-terminal signal peptide or transmembrane domain directing the protein to the cell wall or plasma membrane, respectively, followed by an inhibitor domain preceding the catalytic domain. In contrast, type II PMEs have an N-terminal signal

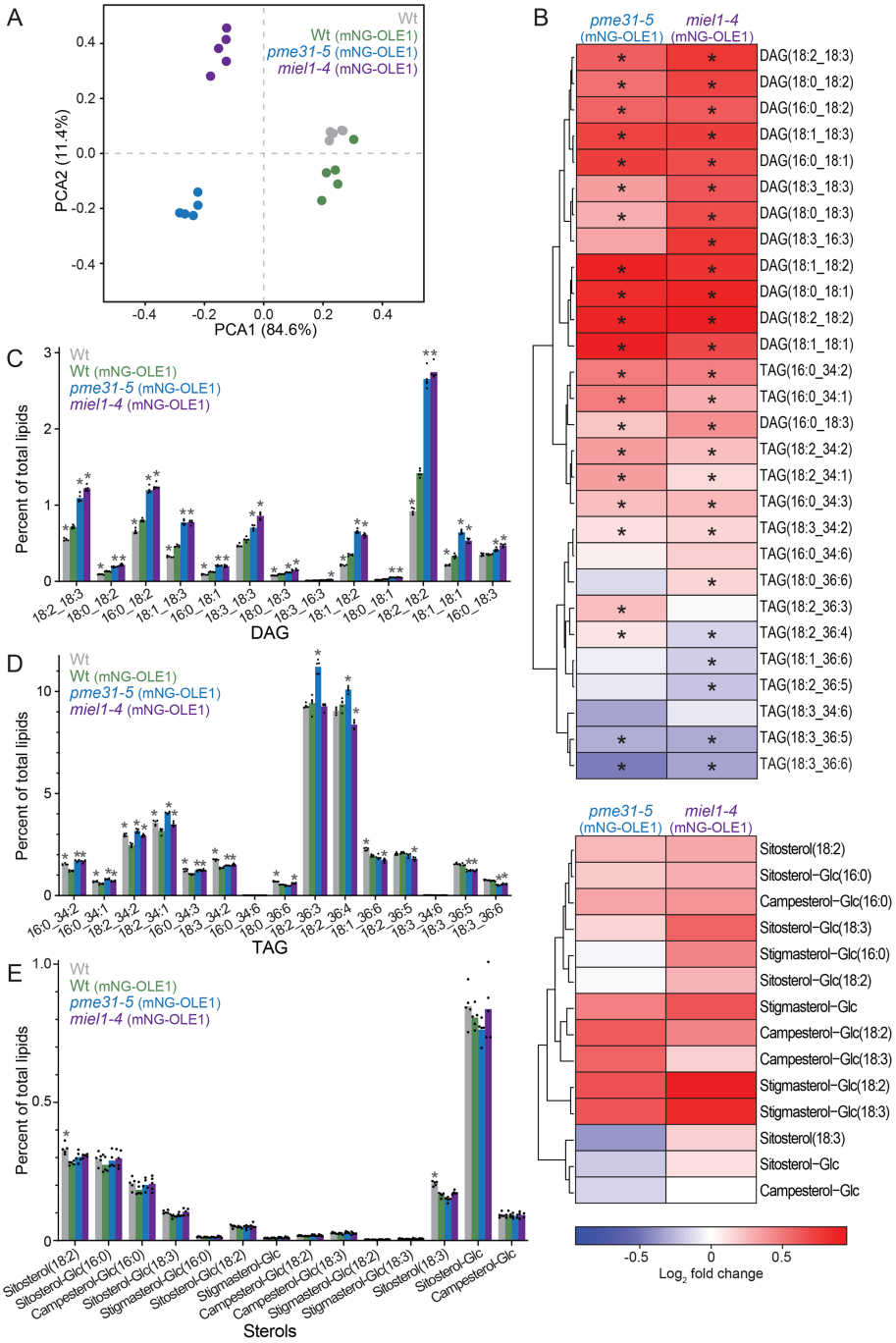

FIGURE 3 | DAG and TAG profiles are altered in *pme31-5* seedlings. (A) PCA analysis of lipidomics data from 2-day-old seedlings shows limited variation among five biological replicates of each genotype. (B) Dendograms and heat maps showing $\log_2$ fold changes in DAG, TAG, and sterol levels in *pme31* and *miel1* mutants relative to Wt (mNG-OLE1). (C–E) Bars show the mean levels of each DAG (C), TAG (D), or sterol (E) species for each genotype plotted as the percent of individual lipid species within the entire sample. *p*-values were generated from Dunnett's multiple comparison tests of individual ANOVA of each lipid species among the five biological replicates (dots). Asterisks in panels (B)–(E) denote values significantly ($p \leq 0.001$) different from Wt (mNG-OLE1).

peptide or transmembrane domain but lack the inhibitor domain (Markovic and Janecek 2004; Gupta et al. 2015). PME31 lacks both the N-terminal localization domain and the inhibitor domain.

To compare the homology of the catalytic domains, we gathered sequences of *Arabidopsis* proteins annotated as PMEs (Tables S1 and S2) and manually truncated the sequences to include the relevant catalytic domains following alignment with PME31. Figure 4 shows a phylogram generated from the catalytic domain alignment (Figure S3). Even though the N-terminal localization and inhibitor domains were not included in the alignment, type I and type II PMEs segregated within the tree into their respective groups, suggesting an evolutionary expansion of the two types of PMEs after their divergence. The PME31 catalytic domain was most similar to type II PMEs (Figure 4), suggesting that PME31 evolved from a type II PME after the divergence of the two types.

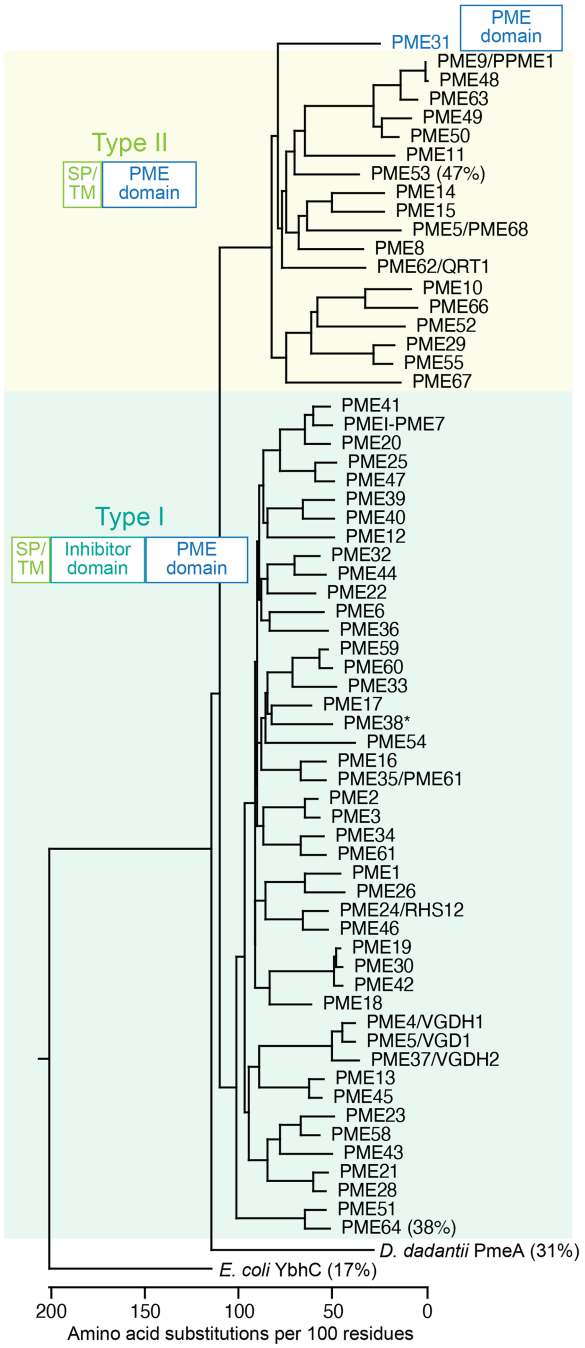

FIGURE 4 | The PME31 catalytic domain is most similar to type II PMEs. Sequences of *Arabidopsis* PME proteins truncated to include only the catalytic domains were aligned with microbial PmeA from *Dickeya dadantii* and YbhC from *E. coli* to generate a phylogenetic tree. The catalytic domains of type I PMEs, which harbor a predicted cleavable signal peptide (SP) or transmembrane (TM) domain and an inhibitor domain on the N-terminus, are distinct from the type II PMEs, which include a SP or TM domain on the N-terminus but lack the inhibitor domain. PME31 lacks both N-terminal domains. The percent identity to PME31 is shown in parentheses for selected proteins. An asterisk marks PME38, a probable pseudogene that groups with type I PMEs and has an inhibitor domain but lacks an N-terminal SP or TM.

The closest type II PME31 relative was PME53, with 47% sequence identity in the catalytic domain (Figure S3). The closest type I relative was PME64, with 38% sequence identity to PME31 (Figure S3).

We aligned the primary sequences of the catalytic domains of PME31, PME53, and PME64 with the well-characterized bacterial PmeA from the plant pathogen *Dickeya dadantii* (Fries et al. 2007) and the *E. coli* YbhC lipase (Eklöf et al. 2009). The alignment (Figure 5) shows that PME31 is generally similar to the other PMEs and the YbhC lipase, which exhibits sequence similarity to PMEs. The catalytically important residues identified in PmeA were conserved in PME31 (Figure 5). Moreover, our various *pme31* alleles, including three isolated in a previous screen (*pme31-1* to *pme31-3*) (Rinaldi et al. 2016), generally impacted conserved amino acids and often altered Gly residues (Figure 5). Additionally, PME31 has a Q rather than an E residue at position 46 in the highly conserved GxYxE motif (Markovic and Janecek 2004) that is present in all other *Arabidopsis* PMEs (Figure S3).

In addition to PME homologs in *Arabidopsis*, PME31 has apparent orthologs throughout the land plant lineage (McCarthy et al. 2014). Many of these orthologs, like PME31, lack N-terminal targeting signals and are much more similar to PME31 than PME31 is to its closest *Arabidopsis* homolog, PME53 (Figure S4A). For example, the monocot *Zea mays* encodes an ortholog with 71% identity to *Arabidopsis* PME31, and the lycophyte *Selaginella moellendorffii* ortholog is 66% identical to *Arabidopsis* PME31 (Figure S4B). One apparently unique feature of the PME31 family is a small insertion at 85–88 amino acids in PME31. This insertion was present in all of the PME31 orthologs examined (Figure S4) but was unique to PME31 in the full alignment of *Arabidopsis* PMEs (Figure S3).

We compared the predicted protein structure of PME31 to its closest type II (PME53) and type I (PME64) *Arabidopsis* relatives and the predicted *D. dadantii* PmeA and *E. coli* YbhC structures (Fries et al. 2007; Eklöf et al. 2009). AlphaFold2 predicted that PME31 would adopt a typical PME structure composed almost entirely of β-strands (Figure 6A). Most of our *pme31* mutations appeared to alter residues on the same face of the protein that harbors the catalytic residues (Figure 6A). As expected from the sequence alignment (Figure 5), the predicted PME31 structure was very similar to those of other PMEs and YbhC, with between 0.57 and 0.71 Å root mean squared deviations (RMSD) across pruned atom pairs (Figure 6B–D).

2.5 | *PME31* Is Expressed in Early Seedling Development

Stored lipid droplet fats are mobilized within the first few days of germinative growth in *Arabidopsis*. We queried previously published global expression data (Klepikova et al. 2016; Waese et al. 2017) to compare the *PME31* temporal expression pattern to genes defective in characterized β-oxidation mutants (Figure S5). These data revealed that the *PME31* transcript is abundant in dry seeds and remains at a reduced level upon the onset of germination (Figure S5A). The *OLE1* transcript, which encodes a lipid droplet coat protein, is also abundant in dry seeds but decreases more dramatically upon germination (Figure S5B). Transcripts of *MIEL1*, which encodes a protein necessary for ubiquitinating OLE1 for degradation, peak during early germination and then decline (Figure S5C). Similarly, *SDP1*, which encodes a TAG lipase, and *PED1*, which encodes a peroxisomal thiolase acting in fatty acid β-oxidation, are more abundant during germination than in dry seeds or after

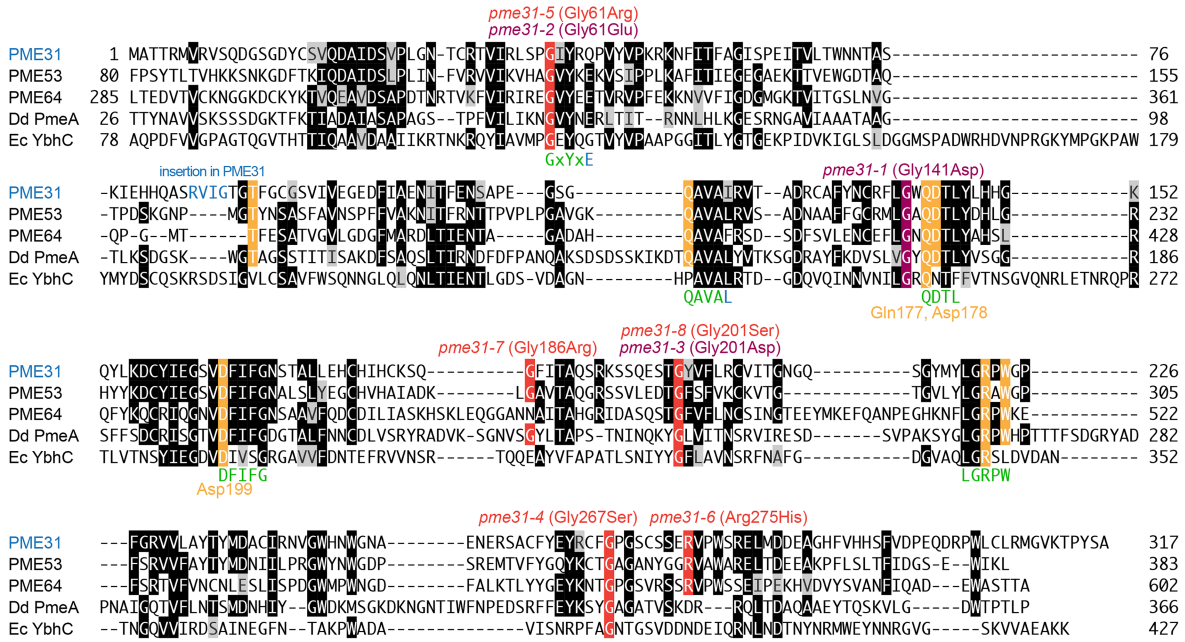

FIGURE 5 | Predicted active-site residues are conserved in PME31 and related enzymes. The alignment shows PME31 aligned with the catalytic domains of its closest type II (PME53) and type I (PME64) *Arabidopsis* homologs, PmeA from *Dickeya dadantii*, and YbhC from *E. coli*. Positions of newly identified mutations (*pme31-4* to *pme31-8*) are highlighted in red and labeled above the alignment, and previously isolated alleles (*pme31-1* to *pme31-3*; Rinaldi et al. 2016) are in maroon. Presumed active site residues, including catalytic residues labeled below the alignment, are highlighted in gold based on *Dickeya dadantii* PmeA (Fries et al. 2007). Five sequence motifs generally conserved in PMEs (Markovic and Janecek 2004) are noted in green below the alignment, with residues altered in PME31 depicted in blue. A short insertion (residues 84–87) in PME31 that is absent in other *Arabidopsis* PMEs is in blue in the PME31 sequence.

germination (Figure 5D, 5E). In contrast, *UBQ10*, often used as a constitutive promoter, maintains relatively consistent mRNA levels from dry seeds to mature leaves (Figure S5F). We concluded that the expression pattern of *PME31* was consistent with a possible role in lipid mobilization during seed germination.

2.6 | A PME31 Reporter Localizes to Peroxisomes After Germination Begins

To investigate where PME31 is localized during lipid mobilization, we examined transgenic plants expressing two reporters: (1) a constitutively expressed red-fluorescent reporter harboring a peroxisomal targeting signal (*pACT2:tdTomato-PTS1*) to visualize peroxisomes and (2) mNeonGreen-tagged PME31 expressed from the *PME31* 5′ regulatory region (*pPME31:PME31-HA-mNeonGreen*) or constitutively expressed untagged mNeonGreen (*pUBQ10:mNeonGreen-HA*). We used confocal microscopy to visualize PME31-HA-mNeonGreen, tdTomato-PTS1, and lipid droplets (stained with MDH). Like the control mNeonGreen-HA (Figure 7A), PME31-HA-mNeonGreen localized to the cytosol and what appeared to be nuclei in stratified seeds and 1-day-old seedlings (Figure 7B). This localization indicates that, unlike other *Arabidopsis* PMEs, PME31 does not traffic to the cell wall. Interestingly, PME31-HA-mNeonGreen localized not only in the cytosol but also with peroxisomes in 2-day-old seedlings (Figure 7B). The same constructs were imaged in hypocotyls from 2- and 3-day-old light-grown seedlings (Figure 7C,D). In hypocotyls, the PME31 reporter was initially cytosolic at 2 days but was largely peroxisome associated in 3-day-old seedlings (Figure 7D). We concluded that PME31 likely localizes in the cytosol and is recruited to peroxisomes during lipid mobilization.

3 | Discussion

The breakdown of lipid droplet triacylglycerols to acetyl-CoA within peroxisomes is essential for germination in *Arabidopsis*. We found that lipid mobilization was impaired in *pme31* mutants, as evidenced by slowed mobilization of lipid droplets (Figure 2A), degradation of oleosin (Figure 2B), and utilization of TAG (Figures 2C,D and 3B,D). These defects were accompanied by elevated DAG levels (Figure 3B,C). These phenotypes, along with some unique features of the catalytic domain of PME31 compared to other PMEs (Figure 4) and abundant *PME31* transcripts in seeds (Figure S5), are consistent with PME31 playing an active role in lipid mobilization during early germination in *Arabidopsis*. Furthermore, a PME31 reporter partially localized to peroxisomes during lipid mobilization (Figure 7), hinting at a direct role for PME31 in peroxisome-associated lipid metabolism.

A role for PME31 in lipid mobilization initially appeared paradoxical. PME31 belongs to a family of at least 64 apparent pectin methylesterases in *Arabidopsis* (Figure 4 and Tables S1 and S2), which typically function in cell wall modification by demethylating pectin (Micheli 2001), a prominent cell wall polymer (Anderson 2016). Indeed, heterologously expressed PME31 displays esterase activity against a pectin substrate in vitro (Dedeurwaerder et al. 2009; Zhang et al. 2023). However, PME31 is less active on pectin in vitro than other

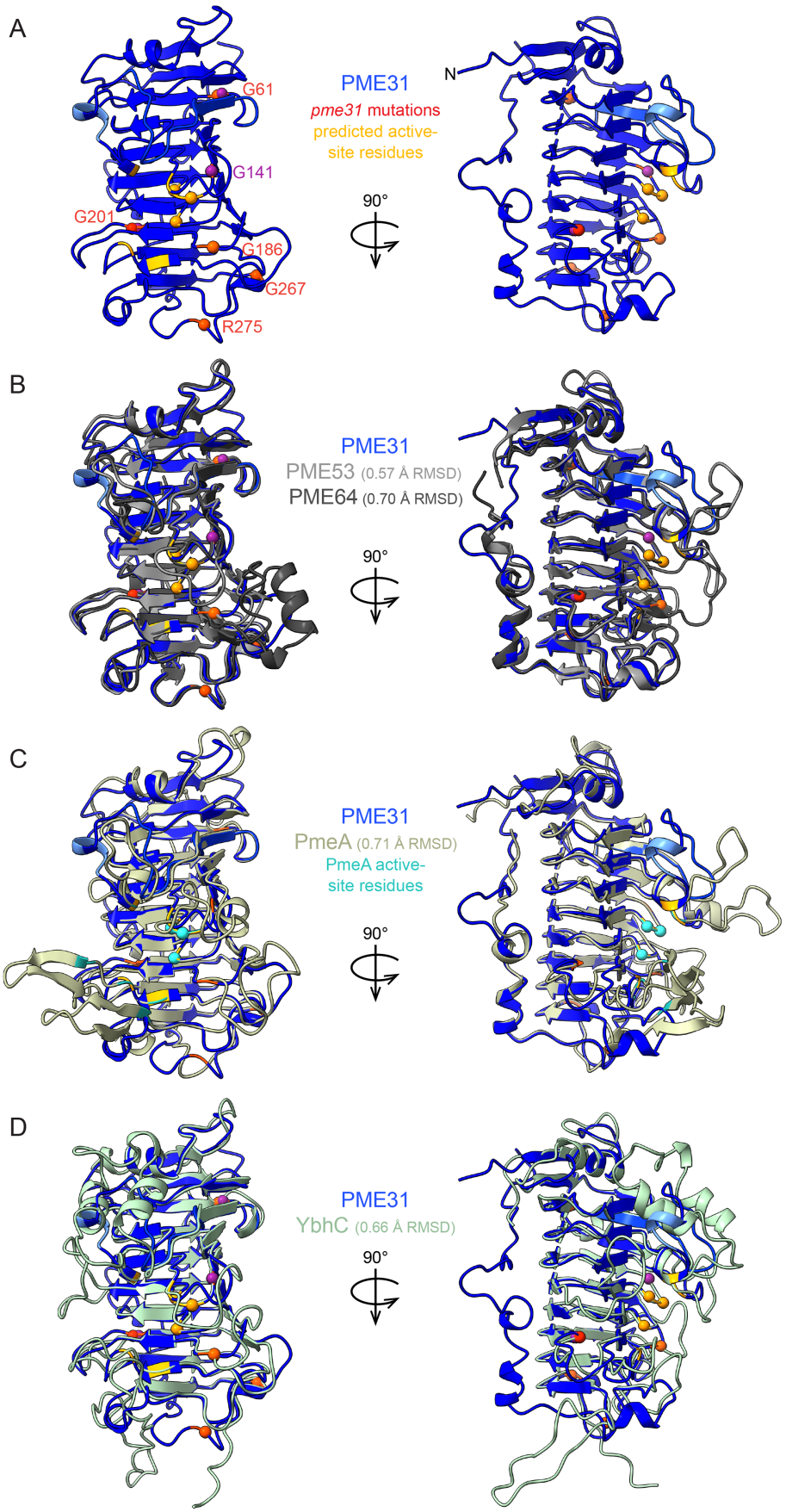

FIGURE 6 | Legend on next page.

FIGURE 6 | The predicted PME31 structure resembles PMEs and YbhC. (A) The PME31 structure was predicted by AlphaFold. Residues altered by *pme31* mutations are highlighted in red (this work) and maroon (Rinaldi et al. 2016). The predicted active site residues from Figure 5 are highlighted in gold, with spheres designating predicted catalytic residues. The small insertion in PME31 that is absent in other *Arabidopsis* PMEs is highlighted in light blue. (B) Alignment of predicted structures of PME31 (blue) with PME53 (gray) and PME64 (charcoal). (C) Alignment of predicted structures of PME31 (blue) and *D. dadantii* PmeA (cream) (Fries et al. 2007). The identified PmeA active site residues are highlighted in teal, with spheres designating catalytic residues. (D) Alignment of the predicted structures of PME31(blue) with *E. coli* YbhC (mint). In B-D, the root mean squared deviations (RMSD) across pruned atom pairs between PME31 and the comparison enzyme are shown in parentheses. The structures on the right in panels (A)–(D) are 90° counterclockwise rotations of the left structure around the vertical axis.

PMEs (Dedeurwaerder et al. 2009). Moreover, unlike PME31, other *Arabidopsis* PMEs harbor N-terminal signal peptides or transmembrane domains that traffic them to the cell wall or plasma membrane (Figure 4 and Tables S1 and S2). In vivo, type I PMEs traverse the secretory system with a co-translationally attached inhibitor domain, which prevents esterase activity before deposition at the cell wall (Wolf et al. 2009). This auto-inhibition may be important because pectin precursors also traverse the secretory system from the Golgi apparatus to the cell wall (Micheli 2001; Anderson 2016). Type II PMEs, in contrast, lack an inhibitor domain but retain a secretion signal. PME31 is notable for being the only *Arabidopsis* PME that lacks both the inhibitor domain and a secretion signal (Figure 4 and Tables S1 and S2). The primary role of PME58, a canonical type I PME expressed during germination, is to modify pectin in seed mucilage (the carbohydrate-rich specialized cell wall of seed coat epidermal cells) and thereby aid in seed hydration and radicle rupture through the seed coat (Hong and Lee 2017). However, the lack of a signal sequence (Figure 4) and the cytosolic localization of a PME31 reporter (Figure 7) would seem to exclude a role for PME31 in mucilage modification. We conclude that PME31 is unlikely to exert its effects through pectin demethylation.

PME31 transcripts are abundant in seeds and remain present during germination (Figure S5; Xiang et al. 2024). A unique role of PME31 during germination is apparent by the isolation of multiple *pme31* mutants from independent forward-genetic screens for sustained lipid droplets (Figure 1) or peroxisomes clustered around sustained lipid droplets (Rinaldi et al. 2016), implying that other *Arabidopsis* PMEs cannot compensate for the lack of PME31. Although *pme31* null mutants germinate like wild type on media lacking ABA, a role for PME31 during germination is further supported by the ABA hypersensitivity of *pme31* seed germination and by the repression of *PME31* transcription by ABI5 (Xiang et al. 2024), a transcription factor that inhibits germination in the presence of ABA (Finkelstein and Lynch 2000; Lopez-Molina and Chua 2000). Intriguingly, MIEL1, which emerged from the same oleosin stabilization screen that yielded PME31, is implicated not only in OLE1 ubiquitination (Traver and Bartel 2023) but also in ABI5 ubiquitination (Nie et al. 2022). It will be interesting to learn the epistatic relationship between *pme31* and *miel1*.

pme31 mutants exhibited some phenotypes characteristic of lipid mobilization mutants, including delayed oleosin degradation and slowed TAG utilization (Figure 2). However, these defects were not sufficiently severe to slow germination (Xiang et al. 2024) or confer sucrose-dependent growth (Figure S1), a defining feature of mutants with more severe lipid mobilization impediments, such as *sdp1* (Eastmond 2006) and *pex12-1* (Kao et al. 2016). Lipidomics analysis revealed that *pme31* seedlings had elevated levels of DAG and some TAG species (Figure 3), indicating a potential reduction in the efficiency of hydrolyzing DAG after TAG hydrolysis. Additionally, *pme31* appeared to have decreased levels of monogalactosyldiacylglycerol (MGDG) (Figure S2). Perhaps impaired lipid mobilization into peroxisomes slows the production of MGDG, which is synthesized via the transfer of D-galactose from UDP-galactose to DAG (Li-Beisson et al. 2013). Similar galactolipid reductions were prominent in the ubiquitin ligase mutant *miel1-4* (Figure S2), suggesting that the lipid profile of *pme31* seedlings may be a hallmark of lipid mobilization defects rather than illuminating the direct catalytic substrate of PME31. *pme31* mutant seedlings are hypersensitive to salt (Yan et al. 2018), and it will be interesting to learn whether this sensitivity relates to the lipid mobilization defects reported here.

Intriguingly, the PME catalytic domain has also been annotated as an acyl-CoA thioester hydrolase YbhC-like domain. In fact, type II PMEs are ambiguously attributed with both a PME domain and an acyl-CoA thioester hydrolase YbhC-like domain (PANTHER 19.0), hinting at a potential role for PME31 in hydrolyzing carboxylic esters in lipid mobilization. This uncertainty in predicted substrate specificity can only be resolved experimentally. For example, the *E. coli* YbhC protein was initially classified as a pectin methylesterase based on sequence similarity but was later reported to have thioester hydrolase activity against palmitoyl-CoA, suggesting activity on a lipid substrate (Kuznetsova et al. 2005). However, subsequent studies provided no evidence supporting esterase activity against either pectin or palmitoyl-CoA, and the in vivo substrate of the *E. coli* YbhC protein remains unclear (Eklöf et al. 2009). Interestingly, the catalytic domain of PME31 is distinct from both type I and type II PMEs (Figures 4 and 5), suggesting that PME31 may also have a distinct catalytic function, including a non-pectin substrate.

PME31 plays a role in lipid mobilization, resulting in delayed utilization of lipids within lipid droplets when PME31 function is interrupted. The localization of a PME31 reporter was consistent with a direct role for PME31 in lipid mobilization during germination. As predicted from the lack of a signal sequence, a PME31 reporter was largely cytosolic in stratified seeds and 1-day-old seedlings. Interestingly, in 2-day-old seedling roots, the PME31 reporter also localized to peroxisomes, the hub of lipid catabolism (Figure 7B). PME31 appeared to be slightly slower to localize to peroxisomes in the hypocotyl (Figure 7D), reinforcing the dynamic nature of this localization. Questions remain about how PME31 associates

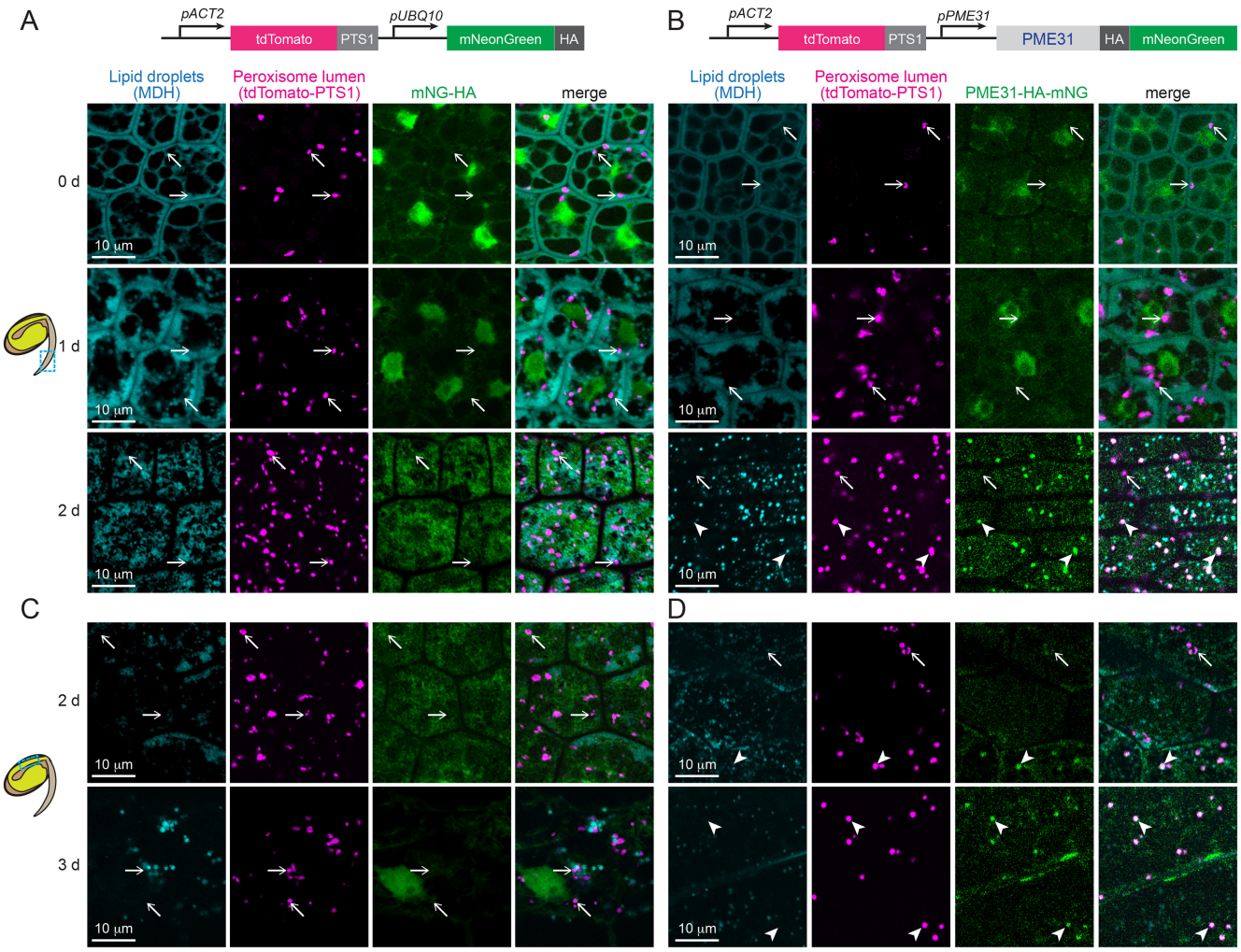

FIGURE 7 | A PME31 reporter localizes to the cytosol and peroxisomes in developing *Arabidopsis* seedlings. Plants expressing a peroxisomal lumenal marker (tdTomato-PTS1, magenta) and free mNeonGreen (mNeonGreen-HA, green) (A, C) or fluorescently tagged PME31 (PME31-HA-mNeonGreen, green) expressed from *PME31* 5′ regulatory sequences (B, D) were imaged in radicles of stratified seeds (0 days) and roots of 1- and 2-day-old light-grown seedlings (A, B) and in hypocotyls of 2- and 3-day-old light-grown seedlings (C, D). Lipid droplets were stained with MDH (cyan); images are single 1-µm slices. PME31-mNeonGreen is cytosolic in younger tissue and becomes more peroxisome associated in older tissues. Arrows mark examples of peroxisomes with minimal mNeonGreen co-localization; arrowheads mark examples of peroxisomes with substantial mNeonGreen co-localization.

with peroxisomes and how this localization is temporally regulated. Although PME31 lacks a canonical peroxisome-targeting signal, some proteins "piggyback" into the peroxisome lumen via association with PTS-containing proteins (Islinger et al. 2009), and others associate with peroxisomes via interaction with peroxisome membrane proteins (Koller et al. 1999; Traver et al. 2022). It will be interesting to learn whether PME31 peripherally associates with peroxisomes or localizes within the lumen and to identify PME31-interacting proteins that mediate this localization.

Although PME31 can demethylate a pectin substrate in vitro (Dedeurwaerder et al. 2009; Zhang et al. 2023), the unique characteristics of PME31 and the phenotypes of PME31-defective plants suggest a different or additional role in vivo. PME31 impacts lipid droplet utilization, which could result from a function as a lipase during lipid mobilization. This hypothesis is further supported by the localization of PME31 to the cytosol (rather than the cell wall) and to peroxisomes as lipids are mobilized. If PME31 has lipase activity, it might assist SDP1 in freeing fatty acids from DAG or MAG. SDP1 is more efficient on TAG than on DAG (Eastmond 2006), and the *pme31* mutant accumulates DAG (Figure 3). However, the *miel1* mutant, defective in a ubiquitin-protein ligase (Traver and Bartel 2023), also accumulates DAG (Figure 3), so DAG accumulation in *pme31* does not indicate a direct role for PME31. Alternatively, if PME31 has acyl-CoA hydrolase activity, it might assist PXA1 in the hydrolysis of fatty acyl-CoAs during peroxisomal import. While PXA1 can hydrolyze the fatty acyl-CoA substrates during import (De Marcos Lousa et al. 2013; Carrier et al. 2019), it is unknown if PXA1 is the only protein performing this function in vivo. Determination of the precise molecular role played by PME31 during lipid utilization at peroxisomes awaits further investigation. PME31 orthologs are present not only in flowering plants but also in mosses (*Physcomitrella patens*) and lycophytes (*Selaginella moellendorffii*) (McCarthy et al. 2014) (Figure S4), and it will be interesting to learn if a lipid-related role for this atypical PME extends throughout land plants.

4 | Materials and Methods

4.1 | Plant Growth Conditions

Plants were grown at 21°C–22°C under continuous white light. Seeds were surface-sterilized in a 3% NaOCl solution with 0.01% Triton X-100, rinsed extensively with water, and stratified by incubating overnight at 4°C in the dark in 0.1% agar. Stratified seeds were plated on plant nutrient (PN) medium (Haughn and Somerville 1986) solidified with 0.6% or 1% (w/v) agar and supplemented with 0.5% (w/v) sucrose (PNS). Seedlings were transferred from plates to soil after 1 week for seed production. For liquid cultures, stratified seeds were grown in 6-well plates containing 3 mL of 6-fold diluted PN supplemented with 0.5% (w/v) sucrose and agitated at 220 rpm on an orbital shaker. For physiological assays monitoring peroxisome function, stratified seeds were pregerminated for 1 day in constant light before sowing on PN solidified with 1% (w/v) agar supplemented with the indicated concentrations of sucrose and/or IBA. After sowing, plates were wrapped in aluminum foil and placed vertically for 4 days at 22°C. Plates were scanned using a flatbed scanner, and hypocotyl lengths were measured using Fiji (version 1.52p).

4.2 | Mutant Isolation

A. thaliana accession Col-0 (Wt) transformed with a *pOLE1:mNeonGreen-OLE1* transgene was mutagenized with ethyl methanesulfonate (EMS) as previously described (Traver and Bartel 2023). Seedlings with delayed degradation of the mNeonGreen-OLE1 reporter (retained fluorescence) following germination were selected, retested, and subjected to whole-genome sequencing as previously described (Traver and Bartel 2023). M_4 progeny of the original screened mutants were used to assay 4-day oleosin retention (Figure 1B) and lipid droplet retention (Figure 2A). Homozygous progeny of the backcrossed *pme31-5* mutant were used for OLE1 and TAG quantification (Figure 2B–D) and lipidomics (Figure 3).

4.3 | Mutant Genotyping

Genotypes of mutants and the presence of various transgenes were determined using PCR with the primers listed in Table S3 of genomic DNA prepared from leaf tissue. DNA was prepared using a modification of a prior protocol (Klimyuk et al. 1993). A cotyledon or small leaf fragment was harvested in a 0.2-mL PCR tube, submerged in 50-mM NaOH, and heated to 99°C for 15 min before adding an equal volume of neutralization buffer (200-mM Tris, 1-mM EDTA, pH 8.0). Amplicons were either assessed by agarose gel electrophoresis (following digestion with the restriction enzymes listed in Table S3 if indicated) or directly sequenced using Sanger sequencing (Genewiz). The *ole1-1* (SM_3_29864) mutant was from the Nottingham *Arabidopsis* Stock Centre.

4.4 | DNA Methods

Inserts for the plant transformation plasmids were constructed in a pUC57-based entry vector via Gibson Assembly (Gibson et al. 2009). To make *pACT2:tdTomato-PTS1, pPME31:PME31-HA-mNG*, 1403 bp of genomic DNA upstream of the *PME31* start codon followed by the *PME31* cDNA fused in frame with an HA tag and the mNeonGreen coding sequences followed by the *HSP18.2* terminator (Nagaya et al. 2010) was inserted into the AvrII restriction site of a pUC57-based entry vector containing *pACT2:tdTomato-PTS1* (Traver and Bartel 2023). This insert was recombined into the pMCS:GW destination vector (Michniewicz et al. 2015) using LR Clonase II (Invitrogen) to make the plant transformation vector. Complete plasmid sequences were verified via Oxford Nanopore reads by Plasmidsaurus (Eugene, OR). Alternative constructs expressing PME31 fused to the C-terminus of a fluorescent reporter resulted in cytosolic protein aggregates and were not pursued further.

4.5 | Plant Transformation

Plasmids were transformed into *Agrobacterium tumefaciens* GV3101 (pMP90) (Koncz and Schell 1986) by electroporation. The transformed Agrobacterium strains were used to transform the Col-0 accession of *A. thaliana* by floral dipping (Clough and Bent 1998). Seedlings harboring the reporter construct were identified by survival on PNS plates supplemented with 10 μg/mL Basta and screening for mNeonGreen fluorescence using a Leica MZ16FA fluorescent stereomicroscope. All selection media were supplemented with 20 μg/mL timentin to prevent Agrobacterium growth. Selected plants were transferred to PNS plates for recovery until being transferred to soil for seed production.

4.6 | Confocal Microscopy

Embryos dissected from stratified seeds and light-grown seedlings were incubated in 100-μM monodansylpentane (MDH) in 50-mM Tris (pH 8) for at least 20 min to stain lipid droplets. The embryos or seedlings were then mounted in lipid droplet dye solution on glass slides (VWR; 48311-950) with 0.16-mm coverslips (VWR; 48393-241) and imaged by live-cell fluorescence confocal microscopy using an Olympus FV3000RS inverted laser scanning confocal microscope equipped with a UPLXAPO 60x/1.42 oil-immersion objective and standard multialkali spectral GaAsP detectors. Images were captured with Fluoview Acquisition software (version 2.4.1.198). tdTomato, MDH, and mNeonGreen were excited with 561, 405, and 488 nm lasers, respectively. tdTomato fluorescence was captured at 570–600 nm. MDH fluorescence was captured at 412–475 nm for Figure 2 and at 430–470 nm for Figure 7. mNeonGreen fluorescence was captured at 500–529 nm (Figures 1 and 2), 500–540 nm (0-, 1-, and 3-day samples for Figure 7), or 500–525 nm (2-day samples in Figure 7). Images were captured using an airy unit of 1.0 with 16-bit depth and a three-track imaging setup, with imaging tracks switching every line. Images were processed in ImageJ/Fiji (version 2.3.0/1.53q).

4.7 | Immunoblotting

Total proteins were harvested from stratified seeds and seedlings grown in the light on PNS. Proteins were extracted

and processed for immunoblotting as previously described (Traver and Bartel 2023). Primary antibodies (mouse anti-HSC70 [1:50000] [Stressgen SPA-817], chicken anti-OLEOSIN [1:2000] [Huang 1992], rabbit anti-OLE1 [1:2000] [Cedarlane, CLAS20-4412], and rabbit anti-ICL [1:1000] [Maeshima et al. 1988]) were incubated overnight at 4°C. Secondary antibodies (diluted 1:2500) were horseradish peroxidase (HRP)-linked goat anti-rabbit antibody (GenScript, A00098), goat anti-chicken (Invitrogen, A16054), and goat anti-mouse (Invitrogen, PI31430). After 1 h of incubation at room temperature with secondary antibodies, membranes were imaged with WesternSure Premium Chemiluminescent substrate (Fisher, 50-489-552) using an Odyssey Fc imaging system (LI-COR, 2801-02).

4.8 | Lipid Analysis

For TLC, lipids were collected from stratified seeds and liquid-grown seedlings via Folch extraction, as previously described (Yu et al. 2021; Traver and Bartel 2023). Samples for each genotype were normalized by seed weight, and replicates within the genotype were normalized by volume during sample collection. Samples were frozen at −80°C and ground on dry ice in 1.7-mL tubes. Lipids were extracted and separated on silica TLC plates as previously described (Traver and Bartel 2023).

For lipidomics, five replicates of 2 mg of 2-day-old light-grown seedlings grown on solid PNS medium topped with filter paper were collected, weighed, and frozen in liquid nitrogen. Samples were processed and quantified by the Kansas Lipidomics Research Center via mass spectrometry (Dataset S1). Lipids with a coefficient of variation less than 0.3 and that were present above the detection limit of 0.0005 nmol for identical samples were used for further analyses.

4.9 | Bioinformatics

Protein sequences were collected for alignments from The *Arabidopsis* Information Resource (TAIR) PhyloGenes (Zhang et al. 2020) for pectin esterases (PTHR31707, classified here as type I PMEs) and acyl-CoA thioester hydrolase YBHC-related proteins (PTHR31321, classified here as type II PMEs). PME31 was collected in the latter group. FASTA sequences were downloaded using the TAIR Sequence Bulk Download Tool for retrieval from the Araport11 protein dataset (Tables S1 and S2). N-terminal transmembrane domains and cleavage sites were detected using Aramemnon 8.1 (Schwacke et al. 2003). The presence of inhibitor domains was evaluated using SMART sequence analysis (Letunic and Bork 2018; Letunic et al. 2021). All proteins except PME31 were manually truncated at their N-termini to remove everything except the PME catalytic domain; PME21 and PME28 were also truncated at their C-termini to remove C-terminal extensions not found in other PMEs. At3g47670, At4g02250, and At1g10770 were excluded from the analysis due to the absence of PME domains, and PME7/PME57 and PME56 were removed due to C-terminal truncations of the catalytic domains. Proteins were aligned using ClustalW with MegAlign (Version 10.0.1 DNASTAR. Madison, WI), and phylogenetic trees were generated from the resultant alignments. Apparent PME31 orthologs were identified from TAIR, and selected orthologs were aligned with PME31 and PME53 as for the PME31 homologs, except that sequences were not trimmed prior to alignment.

RNA-seq data (Klepikova et al. 2016) were collected from ePlant (Waese et al. 2017).

Protein structures were predicted by AlphaFold2 (Jumper et al. 2021; Varadi et al. 2022; Varadi et al. 2024) and imported into UCSF ChimeraX (Meng et al. 2023) for structural alignments. Potential active site residues for PME31 were predicted by alignment with the catalytically annotated PmeA (P0C1A9) from *Dickeya dadantii*. Root mean squared deviations (RMSD) across pruned atom pairs were calculated using UCSF ChimeraX.

4.10 | Quantification, Statistical Analyses, and Data Visualization

Immunoblots and thin-layer chromatograms were quantified using Image Studio Software (version 5.2; LI-COR). Immunoblot signals captured from the Odyssey Fc imaging system were used for quantification. TLC plates were scanned with a flatbed scanner and imported to Image Studio Software as TIFF files, and the green channel was used for quantification.

Percent lipid content lipidomics data were processed in R following the quality control assessment (described above). Lipidomics data were visualized using Rstudio (version 2024.04.1+748) using R version 4.3.0. Data were visualized using the "ggplot2" package in addition to the "corrr," "ggcorrplot," "htmltools," "FactoMineR," and "gplots" packages.

Statistical analyses were performed in GraphPad Prism (version 8.4.3), and figures were assembled in Adobe Illustrator (version 28.0).

Author Contributions

M.S.T., S.H., and B.B. designed the research; S.H. and M.S.T. performed the research; S.H., M.S.T., and B.B. analyzed the data; S.H., B.B., and M.S.T. wrote and revised the manuscript.

Acknowledgments

We thank Ruth Welti and Mary Roth for lipidomics analysis and Nathan Tharp for a modified genomic DNA preparation protocol. We are grateful to Anthony Huang and Masayoshi Maeshima for oleosin and ICL antibodies, respectively. We thank Chelsea An, Gabrielle Buck, Isabella Kreko, DurreShahwar Muhammad, Ana Swearingen, and Nathan Tharp for critical feedback on the manuscript.

Conflicts of Interest

The authors declare no conflicts of interest.

Data Availability Statement

All the data presented in this study can be found in the main manuscript and the supporting information.

Peer Review

The peer review history for this article is available at https://www.webofscience.com/api/gateway/wos/peer-review/10.1002/pld3.70054.

References

Adham, A. R., B. K. Zolman, A. Millius, and B. Bartel. 2005. "Mutations in Arabidopsis Acyl-CoA Oxidase Genes Reveal Distinct and Overlapping Roles in β-Oxidation." *Plant Journal* 41: 859–874.

Anderson, C. T. 2016. "We Be Jammin': An Update on Pectin Biosynthesis, Trafficking and Dynamics." *Journal of Experimental Botany* 67: 495–502.

Carrier, D. J., C. W. T. van Roermund, T. A. Schaedler, et al. 2019. "Mutagenesis Separates ATPase and Thioesterase Activities of the Peroxisomal ABC Transporter, Comatose." *Scientific Reports* 9: 10502.

Choudhary, V., N. Ojha, A. Golden, and W. A. Prinz. 2015. "A Conserved Family of Proteins Facilitates Nascent Lipid Droplet Budding From the ER." *Journal of Cell Biology* 211: 261–271.

Clough, S. J., and A. F. Bent. 1998. "Floral Dip: A Simplified Method for Agrobacterium-Mediated Transformation of *Arabidopsis thaliana*." *Plant Journal* 16: 735–743.

De Marcos Lousa, C., C. W. T. van Roermund, V. L. G. Postis, et al. 2013. "Intrinsic Acyl-CoA Thioesterase Activity of a Peroxisomal ATP Binding Cassette Transporter Is Required for Transport and Metabolism of Fatty Acids." *Proceedings of the National Academy of Sciences* 110: 1279–1284.

Dedeurwaerder, S., L. Menu-Bouaouiche, A. Mareck, P. Lerouge, and F. Guerineau. 2009. "Activity of an Atypical *Arabidopsis thaliana* Pectin Methylesterase." *Planta* 229: 311–321.

Deruyffelaere, C., I. Bouchez, H. Morin, et al. 2015. "Ubiquitin-Mediated Proteasomal Degradation of Oleosins Is Involved in Oil Body Mobilization During Post-Germinative Seedling Growth in Arabidopsis." *Plant & Cell Physiology* 56: 1374–1387.

Deruyffelaere, C., Z. Purkrtova, I. Bouchez, et al. 2018. "PUX10 Is a CDC48A Adaptor Protein That Regulates the Extraction of Ubiquitinated Oleosins From Seed Lipid Droplets in Arabidopsis." *Plant Cell* 30: 2116–2136.

Eastmond, P. J. 2006. "SUGAR-DEPENDENT1 Encodes a Patatin Domain Triacylglycerol Lipase That Initiates Storage Oil Breakdown in Germinating Arabidopsis Seeds." *Plant Cell* 18: 665–675.

Eklöf, J. M., T.-C. Tan, C. Divne, and H. Brumer. 2009. "The Crystal Structure of the Outer Membrane Lipoprotein YbhC From Escherichia Coli Sheds New Light on the Phylogeny of Carbohydrate Esterase Family 8." *Proteins: Structure, Function, and Bioinformatics* 76: 1029–1036.

Finkelstein, R. R., and T. J. Lynch. 2000. "The Arabidopsis Abscisic Acid Response Gene ABI5 Encodes a Basic Leucine Zipper Transcription Factor." *Plant Cell* 12: 599–609.

Footitt, S., S. P. Slocombe, V. Larner, et al. 2002. "Control of Germination and Lipid Mobilization by COMATOSE, the Arabidopsis Homologue of Human ALDP." *EMBO Journal* 21: 2912–2922.

Fries, M., J. Ihrig, K. Brocklehurst, V. E. Shevchik, and R. W. Pickersgill. 2007. "Molecular Basis of the Activity of the Phytopathogen Pectin Methylesterase." *EMBO Journal* 26: 3879–3887.

Fulda, M., J. Schnurr, A. Abbadi, E. Heinz, and J. Browse. 2004. "Peroxisomal Acyl-CoA Synthetase Activity Is Essential for Seedling Development in *Arabidopsis thaliana*." *Plant Cell* 16: 394–405.

Gao, Y., M. L. Skowyra, P. Feng, and T. A. Rapoport. 2022. "Protein Import Into Peroxisomes Occurs Through a Nuclear Pore-Like Phase." *Science* 378: eadf3971.

Gibson, D. G., L. Young, R.-Y. Chuang, J. C. Venter, C. A. Hutchison, and H. O. Smith. 2009. "Enzymatic Assembly of DNA Molecules up to Several Hundred Kilobases." *Nature Methods* 6: 343–345.

Graham, I. A. 2008. "Seed Storage oil Mobilization." *Annual Review of Plant Biology* 59: 115–142.

Gupta, R., P. Kohli, and M. Kalia. 2015. "Pectin Methylesterases: A Review." *Journal of Bioprocessing and Biotechniques* 5: 5.

Haughn, G. W., and C. Somerville. 1986. "Sulfonylurea-Resistant Mutants of *Arabidopsis thaliana*." *Molecular and General Genetics MGG* 204: 430–434.

Hayashi, M., K. Toriyama, M. Kondo, and M. Nishimura. 1998. "2,4-Dichlorophenoxybutyric Acid-Resistant Mutants of Arabidopsis Have Defects in Glyoxysomal Fatty Acid Beta-Oxidation." *Plant Cell* 10: 183–195.

Hong, P. N., and C. Lee. 2017. "Roles of Pectin Methylesterases and Pectin Methylesterase Inhibitors in Plant Physiology." *Journal of Agricultural, Life and Environmental Sciences* 29: 1–17.

Huang, A. H. C. 1992. "Oil Bodies and Oleosins in Seeds." *Annual Review of Plant Biology* 43: 177–200.

Huang, S., Z. Liu, W. Cao, et al. 2022. "The Plant ESCRT Component FREE1 Regulates Peroxisome-Mediated Turnover of Lipid Droplets in Germinating *Arabidopsis* Seedlings." *Plant Cell* 34: 4255–4273.

Islinger, M., K. W. Li, J. Seitz, A. Völkl, and G. H. Lüers. 2009. "Hitchhiking of Cu/Zn Superoxide Dismutase to Peroxisomes—Evidence for a Natural Piggyback Import Mechanism in Mammals." *Traffic* 10: 1711–1721.

Jacquier, N., V. Choudhary, M. Mari, A. Toulmay, F. Reggiori, and R. Schneiter. 2011. "Lipid Droplets Are Functionally Connected to the Endoplasmic Reticulum in *Saccharomyces cerevisiae*." *Journal of Cell Science* 124: 2424–2437.

Jansen, R. L. M., C. Santana-Molina, M. van den Noort, D. P. Devos, and I. J. van der Klei. 2021. "Comparative Genomics of Peroxisome Biogenesis Proteins: Making Sense of the PEX Proteins." *Frontiers in Cell and Development Biology* 9: 654163.

Jumper, J., R. Evans, A. Pritzel, et al. 2021. "Highly Accurate Protein Structure Prediction With AlphaFold." *Nature* 596, no. 7873: 583–589. https://doi.org/10.1038/s41586-021-03819-2.

Kao, Y.-T., W. A. Fleming, M. J. Ventura, and B. Bartel. 2016. "Genetic Interactions Between PEROXIN12 and Other Peroxisome-Associated Ubiquitination Components." *Plant Physiology* 172: 1643–1656.

Kao, Y.-T., K. L. Gonzalez, and B. Bartel. 2018. "Peroxisome Function, Biogenesis, and Dynamics in Plants." *Plant Physiology* 176: 162–177.

Kassan, A., A. Herms, A. Fernández-Vidal, et al. 2013. "Acyl-CoA Synthetase 3 Promotes Lipid Droplet Biogenesis in ER Microdomains." *Journal of Cell Biology* 203: 985–1001.

Klepikova, A. V., A. S. Kasianov, E. S. Gerasimov, M. D. Logacheva, and A. A. Penin. 2016. "A High Resolution Map of the *Arabidopsis thaliana* Developmental Transcriptome Based on RNA-Seq Profiling." *Plant Journal* 88: 1058–1070.

Klimyuk, V. I., B. J. Carroll, C. M. Thomas, and J. D. Jones. 1993. "Alkali Treatment for Rapid Preparation of Plant Material for Reliable PCR Analysis." *Plant Journal* 3: 493–494.

Koller, A., W. B. Snyder, K. N. Faber, et al. 1999. "Pex22p of *Pichia pastoris*, Essential for Peroxisomal Matrix Protein Import, Anchors the Ubiquitin-Conjugating Enzyme, Pex4p, on the Peroxisomal Membrane." *Journal of Cell Biology* 146: 99–112.

Koncz, C., and J. Schell. 1986. "The Promoter of TL-DNA Gene 5 Controls the Tissue-Specific Expression of Chimaeric Genes Carried by a Novel Type of Agrobacterium Binary Vector." *Molecular and General Genetics MGG* 204: 383–396.

Kretzschmar, F. K., L. A. Mengel, A. O. Müller, et al. 2018. "PUX10 Is a Lipid Droplet-Localized Scaffold Protein That Interacts With CELL DIVISION CYCLE48 and Is Involved in the Degradation of Lipid Droplet Proteins." *Plant Cell* 30: 2137–2160.

Kumar, R., M. Islinger, H. Worthy, R. Carmichael, and M. Schrader. 2024. "The Peroxisome: An Update on Mysteries 3.0." *Histochemistry and Cell Biology* 161: 99–132.

Kuznetsova, E., M. Proudfoot, S. A. Sanders, et al. 2005. "Enzyme Genomics: Application of General Enzymatic Screens to Discover New Enzymes." *FEMS Microbiology Reviews* 29: 263–279.

Letunic, I., and P. Bork. 2018. "20 Years of the SMART Protein Domain Annotation Resource." *Nucleic Acids Research* 46: D493–D496.

Letunic, I., S. Khedkar, and P. Bork. 2021. "SMART: Recent Updates, New Developments and Status in 2020." *Nucleic Acids Research* 49: D458–D460.

Li-Beisson, Y., B. Shorrosh, F. Beisson, et al. 2013. "Acyl-Lipid Metabolism." *Arabidopsis Book* 11: e0161.

Lingard, M. J., M. Monroe-Augustus, and B. Bartel. 2009. "Peroxisome-Associated Matrix Protein Degradation in Arabidopsis." *Proceedings of the National Academy of Sciences* 106: 4561–4566.

Lopez-Molina, L., and N.-H. Chua. 2000. "A Null Mutation in a bZIP Factor Confers ABA-Insensitivity in *Arabidopsis thaliana*." *Plant & Cell Physiology* 41: 541–547.

Maeshima, M., H. Yokoi, and T. Asahi. 1988. "Evidence for no Proteolytic Processing During Transport of Isocitrate Lyase Into Glyoxysomes in Castor Bean Endosperm." *Plant & Cell Physiology* 29: 381–384.

Markovic, O., and S. Janecek. 2004. "Pectin Methylesterases: Sequence-Structural Features and Phylogenetic Relationships." *Carbohydrate Research* 339: 2281–2295.

McCarthy, T. W., J. P. Der, L. A. Honaas, C. W. dePamphilis, and C. T. Anderson. 2014. "Phylogenetic Analysis of Pectin-Related Gene Families in *Physcomitrella patens* and Nine Other Plant Species Yields Evolutionary Insights Into Cell Walls." *BMC Plant Biology* 14: 79.

Meng, E. C., T. D. Goddard, E. F. Pettersen, et al. 2023. "UCSF ChimeraX: Tools for Structure Building and Analysis." *Protein Science* 32: e4792.

Micheli, F. 2001. "Pectin Methylesterases: Cell Wall Enzymes With Important Roles in Plant Physiology." *Trends in Plant Science* 6: 414–419.

Michniewicz, M., E. M. Frick, and L. C. Strader. 2015. "Gateway-Compatible Tissue-Specific Vectors for Plant Transformation." *BMC Research Notes* 8: 63.

Nagaya, S., K. Kawamura, A. Shinmyo, and K. Kato. 2010. "The HSP Terminator of Arabidopsis Thaliana Increases Gene Expression in Plant Cells." *Plant & Cell Physiology* 51: 328–332.

Nie, K., H. Zhao, X. Wang, Y. Niu, H. Zhou, and Y. Zheng. 2022. "The MIEL1-ABI5/MYB30 Regulatory Module Fine Tunes Abscisic Acid Signaling During Seed Germination." *Journal of Integrative Plant Biology* 64: 930–941.

Quettier, A.-L., and P. J. Eastmond. 2009. "Storage oil Hydrolysis During Early Seedling Growth." *Plant Physiology and Biochemistry* 47: 485–490.

Ravindran, R., I. O. L. Bacellar, X. Castellanos-Girouard, et al. 2023. "Peroxisome Biogenesis Initiated by Protein Phase Separation." *Nature* 617: 608–615.

Rinaldi, M., A. Patel, J. Park, K. Lee, L. Strader, and B. Bartel. 2016. "*Arabidopsis thaliana* Mutants With Altered Seedling Peroxisome Size or Distribution Reveal Genes Important for Peroxisomal Metabolism." *Genetics* 204: 1089–1115.

Rylott, E. L., P. J. Eastmond, A. D. Gilday, et al. 2006. "The *Arabidopsis thaliana* Multifunctional Protein Gene (MFP2) of Peroxisomal Beta-Oxidation Is Essential for Seedling Establishment." *Plant Journal* 45: 930–941.

Schwacke, R., A. Schneider, E. van der Graaff, et al. 2003. "ARAMEMNON, a Novel Database for Arabidopsis Integral Membrane Proteins." *Plant Physiology* 131: 16–26.

Skowyra, M. L., P. Feng, and T. A. Rapoport. 2024. "Towards Solving the Mystery of Peroxisomal Matrix Protein Import." *Trends in Cell Biology* 34: 388–405.

Thazar-Poulot, N., M. Miquel, I. Fobis-Loisy, and T. Gaude. 2015. "Peroxisome Extensions Deliver the Arabidopsis SDP1 Lipase to Oil Bodies." *Proceedings of the National Academy of Sciences* 112: 4158–4163.

Theodoulou, F. L., and P. J. Eastmond. 2012. "Seed Storage Oil Catabolism: A Story of Give and Take." *Current Opinion in Plant Biology* 15: 322–328.

Traver, M. S., and B. Bartel. 2023. "The Ubiquitin-Protein Ligase MIEL1 Localizes to Peroxisomes to Promote Seedling Oleosin Degradation and Lipid Droplet Mobilization." *Proceedings of the National Academy of Sciences* 120: e2304870120.

Traver, M. S., S. E. Bradford, J. L. Olmos, et al. 2022. "The Structure of the Arabidopsis PEX4-PEX22 Peroxin Complex—Insights Into Ubiquitination at the Peroxisomal Membrane." *Frontiers in Cell and Development Biology* 10: 838923.

Varadi, M., S. Anyango, M. Deshpande, et al. 2022. "AlphaFold Protein Structure Database: Massively Expanding the Structural Coverage of Protein-Sequence Space With High-Accuracy Models." *Nucleic Acids Research* 50: D439–D444.

Varadi, M., D. Bertoni, P. Magana, et al. 2024. "AlphaFold Protein Structure Database in 2024: Providing Structure Coverage for Over 214 Million Protein Sequences." *Nucleic Acids Research* 52: D368–D375.

Waese, J., J. Fan, A. Pasha, et al. 2017. "ePlant: Visualizing and Exploring Multiple Levels of Data for Hypothesis Generation in Plant Biology." *Plant Cell* 29: 1806–1821.

Walther, T. C., J. Chung, and R. V. Farese. 2017. "Lipid Droplet Biogenesis." *Annual Review of Cell and Developmental Biology* 33: 491–510.

Wiszniewski, A. A. G., J. D. Bussell, R. L. Long, and S. M. Smith. 2014. "Knockout of the Two Evolutionarily Conserved Peroxisomal 3-Ketoacyl-CoA Thiolases in Arabidopsis Recapitulates the Abnormal Inflorescence Meristem 1 Phenotype." *Journal of Experimental Botany* 65: 6723–6733.

Wolf, S., T. Rausch, and S. Greiner. 2009. "The N-Terminal Pro Region Mediates Retention of Unprocessed Type-I PME in the Golgi Apparatus." *Plant Journal* 58: 361–375.

Xiang, Y., C. Zhao, Q. Li, et al. 2024. "Pectin Methylesterase 31 Is Transcriptionally Repressed by ABI5 to Negatively Regulate ABA-Mediated Inhibition of Seed Germination." *Frontiers in Plant Science* 15: 1336689.

Yan, J., H. He, L. Fang, and A. Zhang. 2018. "Pectin Methylesterase31 Positively Regulates Salt Stress Tolerance in Arabidopsis." *Biochemical and Biophysical Research Communications* 496: 497–501.

Yu, L., J. Fan, C. Zhou, and C. Xu. 2021. "Sterols Are Required for the Coordinated Assembly of Lipid Droplets in Developing Seeds." *Nature Communications* 12: 5598.

Zhang, P., T. Z. Berardini, D. Ebert, et al. 2020. "PhyloGenes: An Online Phylogenetics and Functional Genomics Resource for Plant Gene Function Inference." *Plant Direct* 4: e00293.

Zhang, X., H. Guo, C. Xiao, et al. 2023. "PECTIN METHYLESTERASE INHIBITOR18 Functions in Stomatal Dynamics and Stomatal Dimension." *Plant Physiology* 192: 1603–1620.

Zolman, B. K., I. D. Silva, and B. Bartel. 2001. "The Arabidopsis pxa1 Mutant Is Defective in an ATP-Binding Cassette Transporter-Like Protein Required for Peroxisomal Fatty Acid β-Oxidation." *Plant Physiology* 127: 1266–1278.

Supporting Information

Additional supporting information can be found online in the Supporting Information section.